Extended Data

Colistin-resistant bacteria poses few risks under physiological conditions

Toyotaka Sato, Soh Yamamoto, Masaru Usui, Noriko Ogasawara,

Wataru Hayashi, Masato Suzuki, Noriyuki Nagano,

Chie Nakajima, Yasuhiko Suzuki, Motohiro Horiuchi,

Satoshi Takahashi, Shin-ichi Yokota, Yutaka Tamura

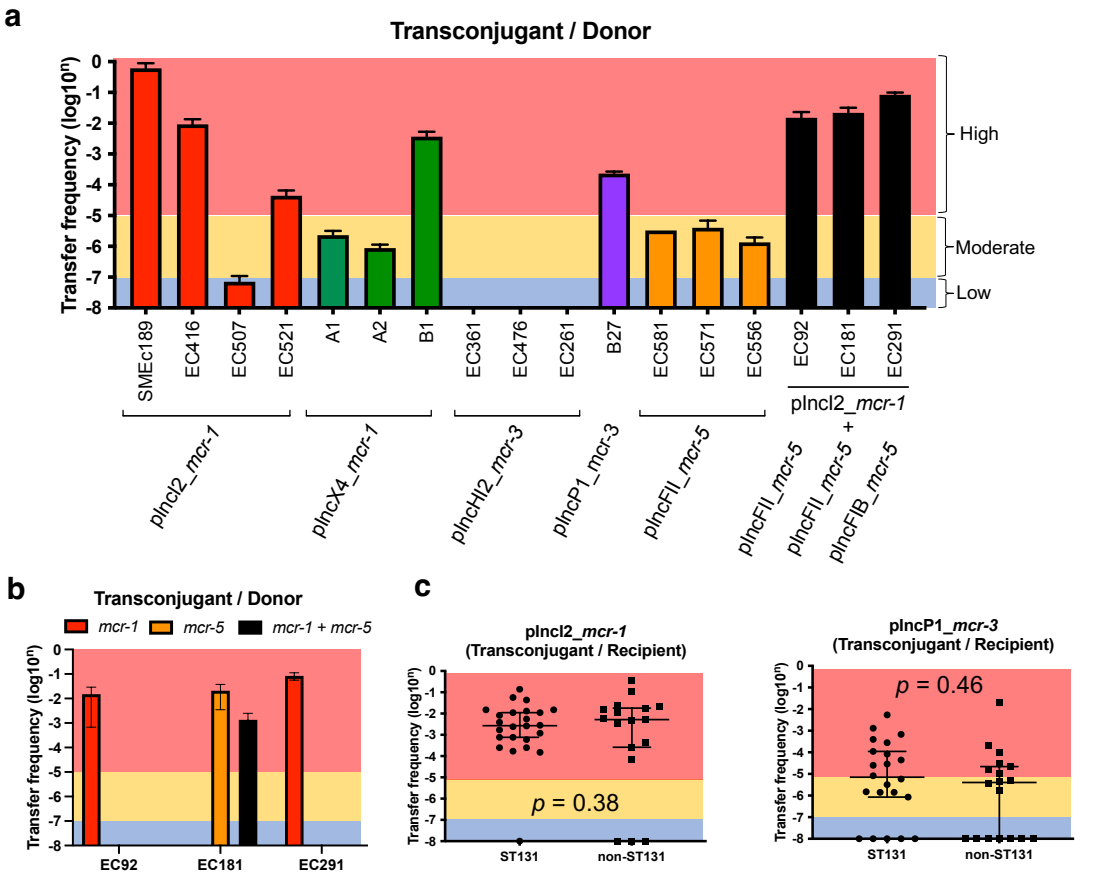

Extended Data Fig. 1 | Transfer and recipient abilities of plasmid-mediated colistin resistance determinants in *E. coli* ST131. (a) Transfer frequencies of *mcr-1*-, *mcr-3*-, and *mcr-5*-harbouring plasmids from various *E. coli* donors to *E. coli* ST131. pIncI2_*mcr-1*-, pIncX4_*mcr-1*-, pIncHI2_*mcr-3*-, pIncP1_*mcr-3*-, and pIncFII_*mcr-5*-harbouring *E. coli* donors and the recipient *E. coli* ST131 strain [colistin-susceptible, with a colistin minimum inhibitory concentration (MIC) of 0.5 mg/L], SME98, were used. Three donors (EC92, EC181, and EC291) possessed multiple *mcr* plasmids. The plasmid pIncI2_*mcr-1*, which was present in three donors (*E. coli* SMEc189, EC416, and EC521), exhibited a high transfer frequency (> 1 x 10^{-5}, meaning more than 1 of in 10^5 donor clones transferred the *mcr*-harbouring plasmid to the recipient). High transfer frequencies were also observed for pIncX4_*mcr-1* and from pIncP1_*mcr-3* in one donor each (B1 and B27, respectively). Frequent loss of pIncX4_*mcr-1* from SME98 after the transfer was observed during subcultivation in the absence of colistin. None of the three donors carrying pIncHI2_*mcr-3* transferred *mcr-3*. The transfer frequencies of pIncFII_*mcr-5* were moderate, ranging from 10^{-7} to 10^{-5}. After obtaining the transconjugant, we identified the transfer frequency of each *mcr* and a recipient marker by PCR; at least 16 colonies grew on MHII agar containing 2 mg/L of colistin and 1 mg/L of ciprofloxacin. (b) Transfer frequencies of multiple *mcr*-harbouring plasmids from three donors (EC92, EC181, and EC291) into *E. coli* ST131. The transfer frequencies of plasmids in donors coharbouring pIncI2_*mcr-1* and pIncFII_*mcr-5* were dependent on the donor isolate; *E. coli* EC92 and EC291 transferred only pIncI2_*mcr-1*, whereas EC181 transferred both plasmids. (c) Comparison of the transfer frequency of *mcr*-harboring plasmids between ST131 (n = 22) and non-ST131 (n = 18) fluoroquinolone-resistant *E. coli* recipient isolates. We used *E. coli* EC92 and B27 as donors of pIncI2_*mcr-1* and pIncP1_*mcr-3*, respectively, because of their high transfer abilities. Geometric means with geometric standard deviations are indicated.

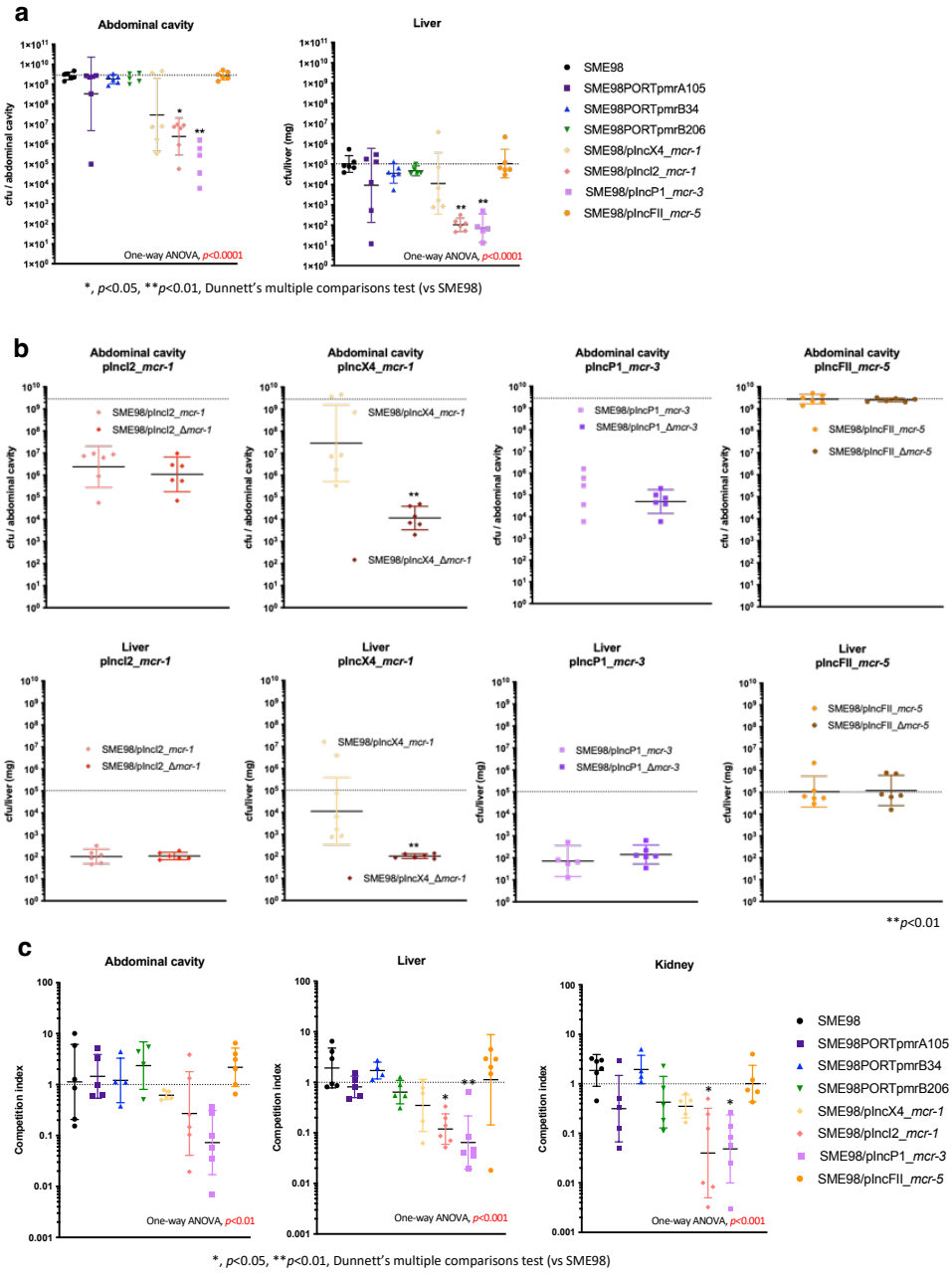

Extended Data Fig. 2 | Effect of the acquisition of colistin resistance determinants in a murine infection model. (a) Number of viable bacteria for colistin-resistant *E. coli* ST131 mutants after infection in mice. We evaluated the number of viable bacteria for SME98 and its colistin-resistant mutants in the abdominal cavity and liver at 16 h after infection (intraperitoneal infection with 2.5 x 10^4 cfu/mouse with 2.5% porcine mucin). (b) Comparison of the number of viable bacteria for plasmid-mediated colistin-resistant SME98 mutants and their *mcr*-deletion mutants. The conditions used for the infections were the same as described in (a). (c). Competition assay in a murine infection model. A rifampicin-resistant SME98 (SME98RIF) strain and colistin-resistant SME98 mutants were mixed and used to infect mice (intraperitoneal infection with 5.0 x 10^2 cfu each/mouse with 2.5% porcine mucin). The number of viable bacteria for SME98RIF and colistin-resistant SME98 mutants on agar containing rifampicin (for SME98RIF) or ciprofloxacin (total numbers of bacteria obtained for SME98) was calculated at 48 h after infection. The competitive index was calculated as [(cfus of colistin-resistant SME98)/(cfus of SME98RIF)]. Geometric means with geometric standard deviations are indicated.

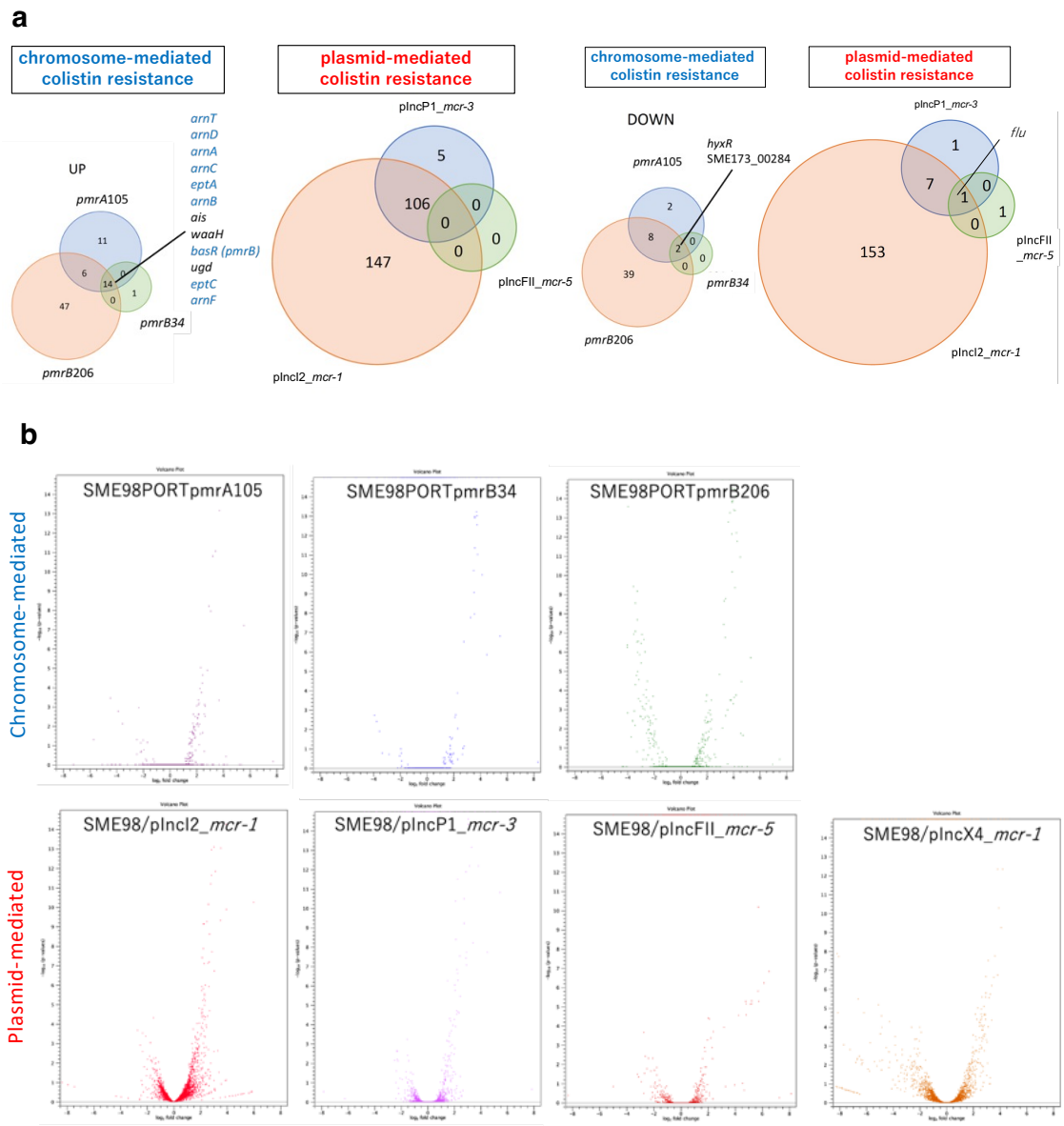

Extended Data Fig. 3 | Transcriptome profiles after the acquisition of colistin resistance determinants in *E. coli* ST131. (a) The number of up- (left) or down- (right) regulated genes in colistin-resistant SME98 mutants. The transcript levels of chromosome-mediated colistin-resistant SME98 mutants [SME98PORTpmrA105 (*pmrA*), SME98PORTpmrB34 (*pmrB*34), and SME98PORTpmrB206 (*pmrB*206)] and plasmid-mediated colistin-resistant SME98 mutants [SME98/pIncI2_*mcr-1* (pIncI2_*mcr-1*), SME98/pIncP1_*mcr-3* (pIncP1_*mcr-3*), and SME98/pIncFII_*mcr-5* (pIncFII_*mcr-5*)] were compared with those of SME98 by RNA-Seq. The values indicate the number of genes whose expression changed significantly compared to that in SME98 (4-fold up- or downregulated vs. SME98, FDR*p* <0.05). (b) Volcano plots of chromosome- and plasmid-mediated colistin resistance. The X-axis shows the fold changes of transcripts, and the Y-axis shows the p values of the changes (vs. SME98). The results of RNA-Seq analyses are shown as the average of duplicate biological samples (different lots of MHBII were used for each sample).

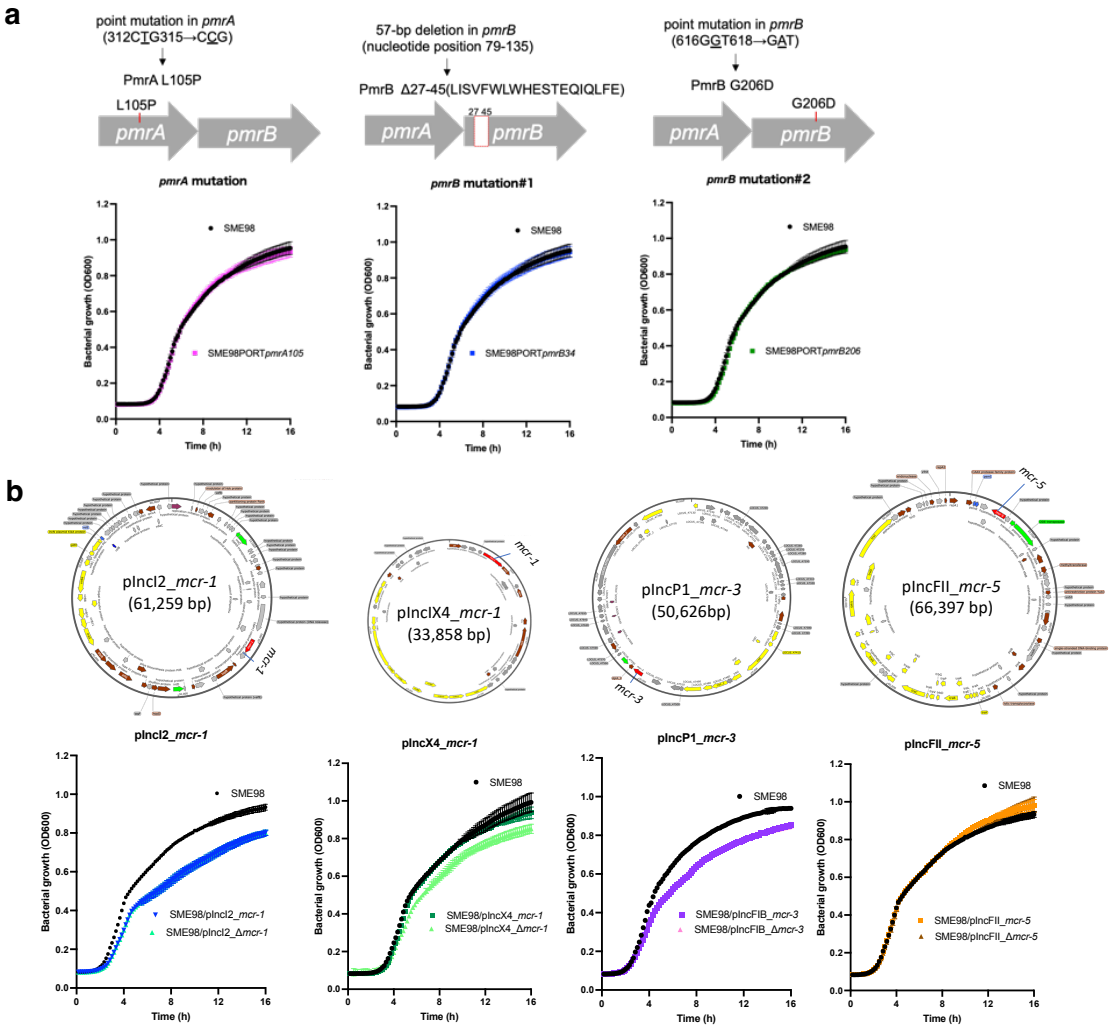

Extended Data Fig. 4 | Bacterial growths of *E. coli* ST131 mutants after the acquisition of colistin resistance determinants. *E. coli* SME98 was used as a parent ST131 strain. (a) Bacterial growth of chromosome-mediated colistin-resistant *E. coli* ST131 mutants. *pmrA* or *pmrB* mutations were introduced into SME98 (SME98PORTpmrA105, SME98PORTpmrB34, and SME98PORTpmrB206). These bacteria were cultured in MHBII at 140 rpm and 37°C for 16 h, and growth was monitored as turbidity (OD_{600})[18]. (b) Bacterial growth of plasmid-mediated colistin-resistant *E. coli* ST131 mutants. pIncI2_*mcr-1*, pIncX4_*mcr-1*, pIncP1_*mcr-3*, and pIncFII_*mcr-5* were transferred from donors (EC92, B1, B27, and EC181, respectively) to SME98 by broth mating. The bacterial growth of these transconjugants (SME98/pIncI2_*mcr-1*, SME98/pIncX4_*mcr-1*, SME98/pIncP1_*mcr-3*, and SME98/pIncFII_*mcr-5*, respectively) and their *mcr* deletion mutants was monitored (OD_{600}). Arrows in the plasmid maps show the gene encoding *mcr* (red), functional proteins (brown), transposons/integrons (green), transferred genes (yellow), and hypothetical proteins (grey).

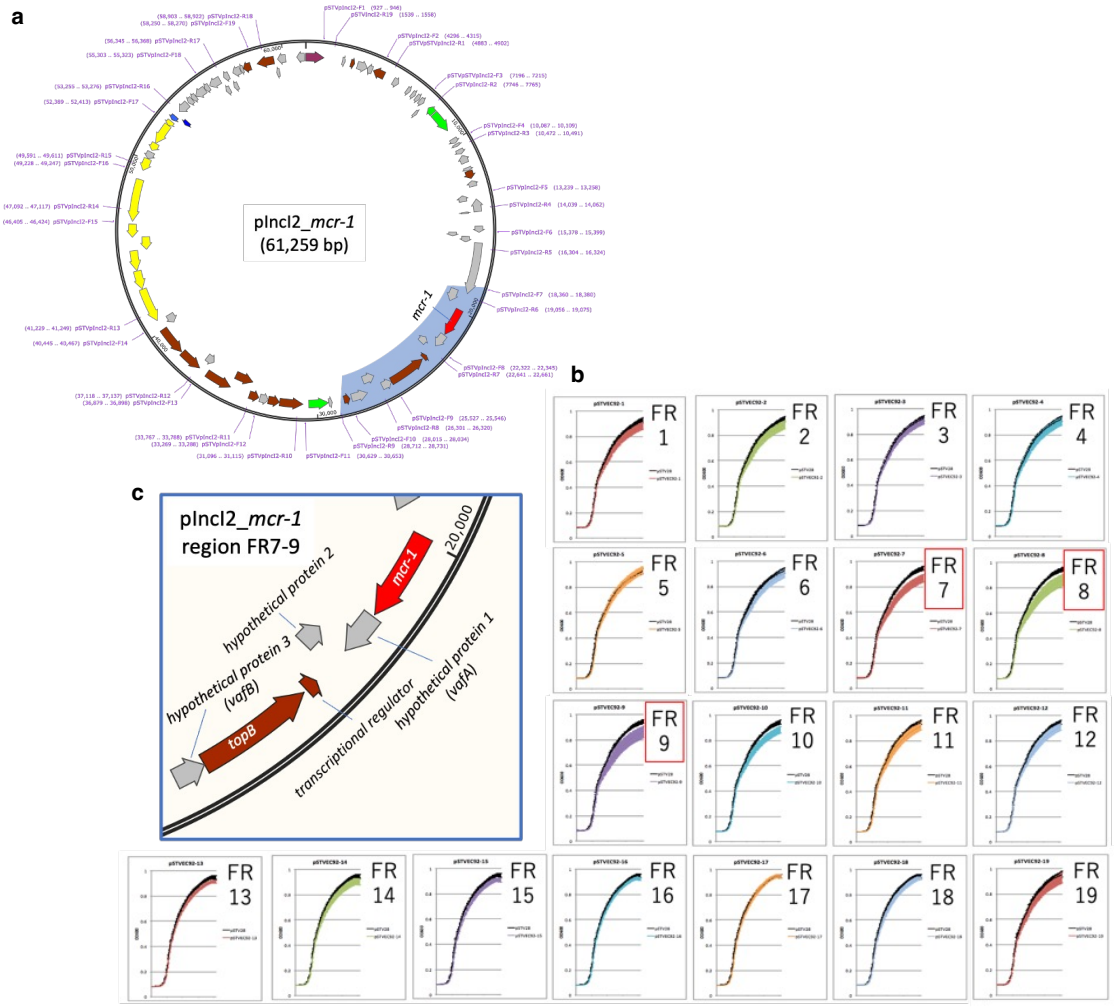

Extended Data Fig. 5 | Identification of regions in the pIncI2_*mcr-1* plasmid that affect the bacterial growth of ST131. (a) Map of pIncI2_*mcr-1* and primer pairs for cloning its 19 fragments. pIncI2_*mcr-1* derived from *E. coli* EC92 was used. Arrows in the plasmid map show the genes encoding *mcr-1* (red), functional proteins (brown), transposons/integrons (green), transferred genes (yellow), and hypothetical proteins (grey). We divided pIncI2_*mcr-1* into an average of 19 3.2 kb DNA fragments [each fragment contained the whole sequence of the coding region with the putative promoter region (upstream 500 bp)]. We then cloned each fragment into the pSTV28 vector and introduced the constructs into SME98, and bacterial growth was monitored. Purple shows the primer annealing regions for amplification and cloning of the 19 DNA fragments into pSTV28 (primer sequences are listed in Table S6). The blue highlighting shows the regions from FR7 to FR9. (b) Influence of the 19 DNA fragments derived from pIncI2_mcr-1 on the bacterial growth of *E. coli* ST131. The 19 DNA fragments from pIncI2_*mcr-1* were cloned into pSTV28 and electroporated into the SME98 strain. The bacterial growth of SME98 (black) and fragment-containing SME98 mutants (coloured) was monitored at OD_{600}. (c) Genes present in the regions from FR7 to FR9 of pIncI2_*mcr-1*.

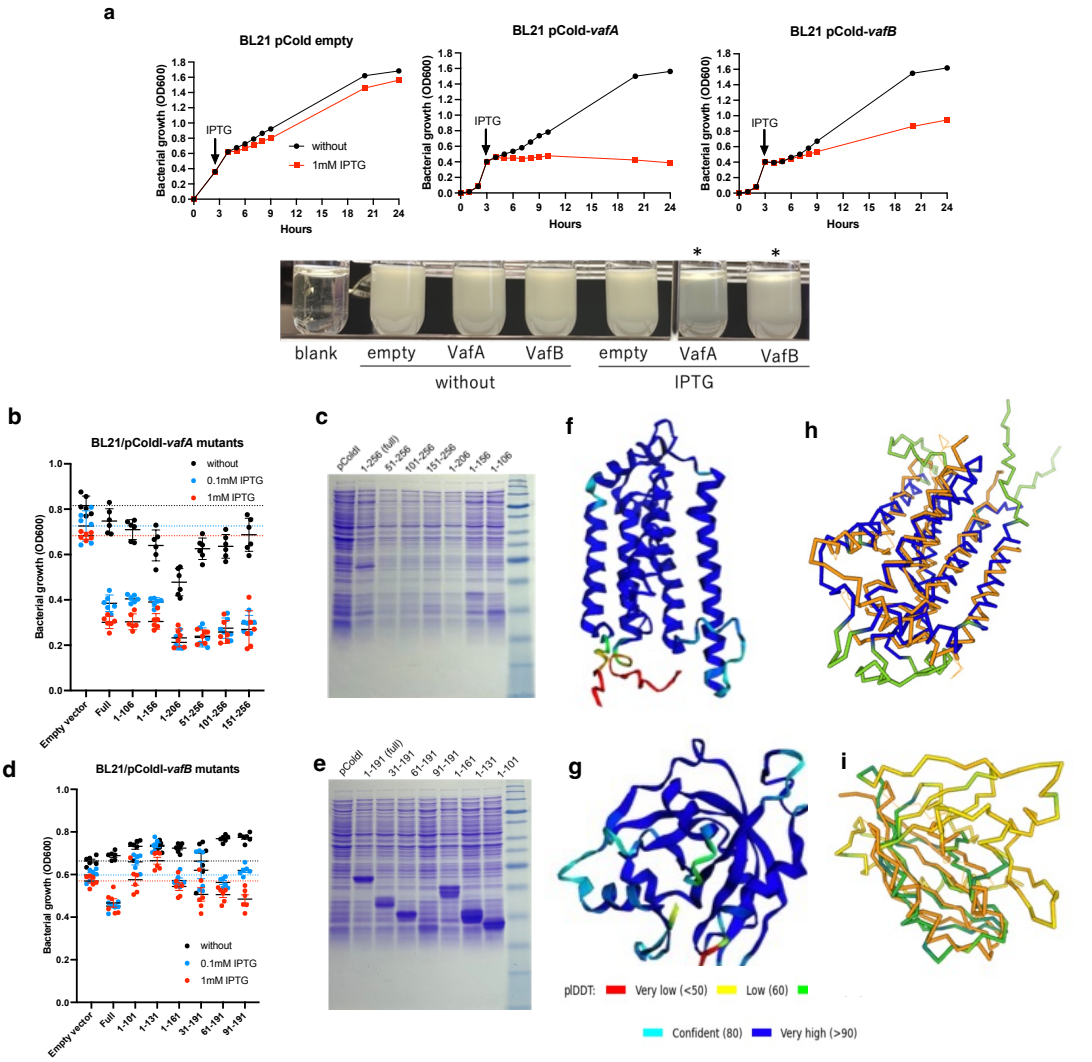

Extended Data Fig. 6 | Expression of VafA/VafB and the flanking mutants in *E. coli* BL21. (a) Bacterial growth of *E. coli* BL21 expressing VafA or VafB. pCold-vafA and pCold-vafB were constructed to strictly control VafA and VafB expression in *E. coli* BL21 via induction with 1 mM IPTG at 12°C, because expression of VafA under pSTV28 could not be maintained during cultivation in SME98 (the sequence of *vafA* was disrupted and/or mutated), and we hypothesized that *vafA* is toxic in *E. coli*. Bacterial growth was monitored as the turbidity of the medium (OD_{600}). The figure shows the bacterial growth after 24 h of cultivation. **p* <0.05 vs. empty vector. (b and d) The bacterial growth of flank-*vafA* (b) and flank-*vafB* (d) *E. coli* BL21 containing the pCold-I vector harbouring *vafA* or *vafB* and their flanking mutants after induction with 0.1 or 1 mM IPTG and monitoring of bacterial growth (OD_{600}). (c and e) The pCold-based protein expression profiles in whole-cell lysates were examined by SDS-PAGE with Coomassie Brilliant Blue staining. The numbers in (b)-(e) show the amino acid positions of each flanking mutant of VafA or VafB. (f, g) Predicted structural models of VafA and BafB. The protein structures of VafA (f) and VafB (g) were predicted using ColabFold v1. 5.2. The per-residue confidence scores (pIDDT) of the predicted structural models are shown with the indicated colors (red, yellow, green, cyan, or blue). AlphaFold2-predicted structural models of VafA (blue and green) and VafB (yellow and green) and structural comparison with phosphatidylglycerol-phosphatase B of *Bacillus subtilis* (PDB: 2NRA, blue) and elongation factor 1-alpha of *Saccharomyces cerevisiae* (PDB: 1IJE, orange), respectively (h and i). The Z score, root mean square deviation (RMSD), and amino acid identity (AA %ID) were 15.4, 3.6, and 11 for VafA, and 5.6, 3.0, and 7 for VafB, respectively.

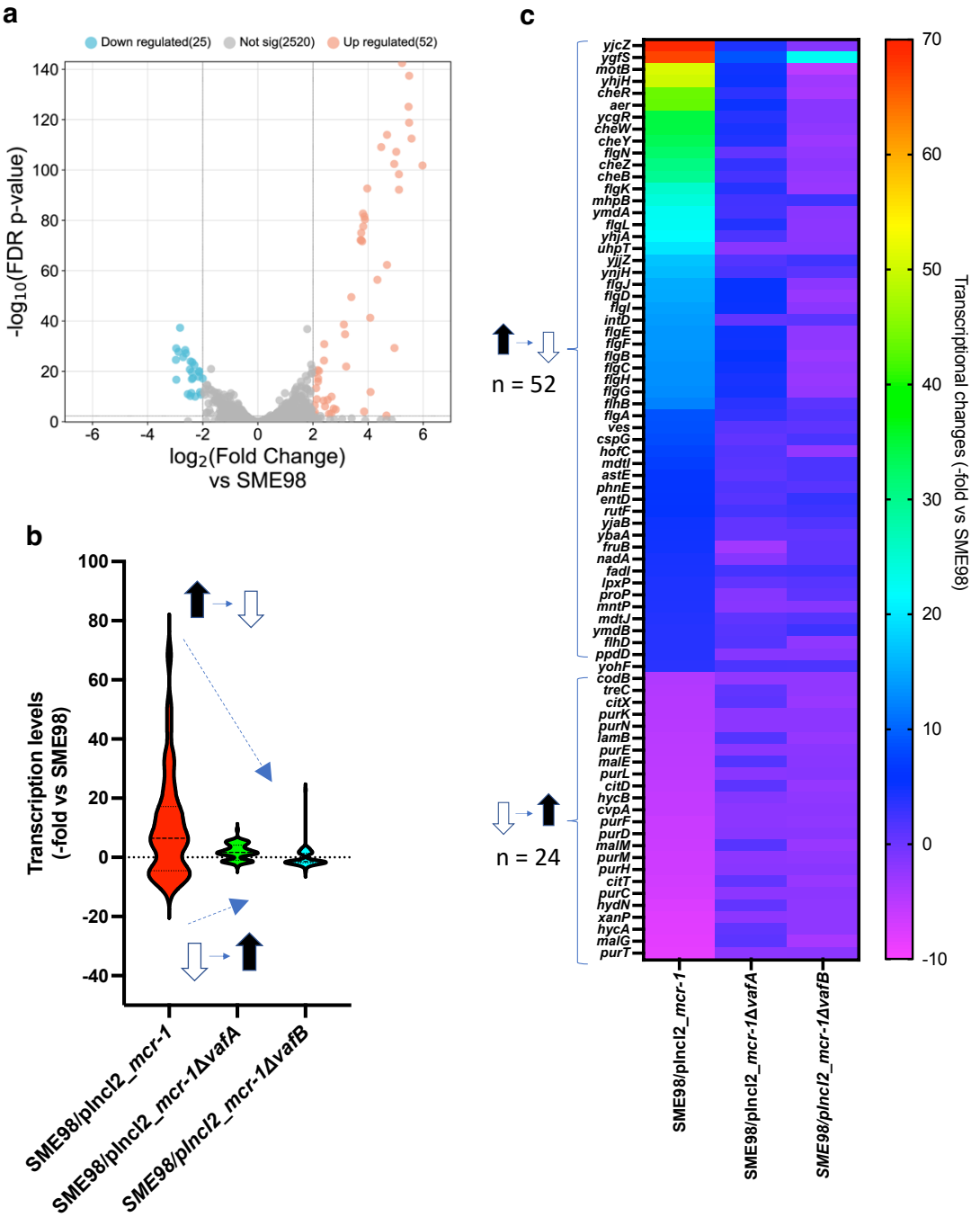

Extended Data Fig. 7 | Screening for up- or down-regulated genes after deletion of *vafA* and *vafB* in *E. coli*. (a) Significantly up- or downregulated genes after acquisition of pIncI2_*mcr-1* in *E. coli* ST131 SME98. The 486 significantly up- or downregulated genes (vs. SME98; and FDR*p* <0.005) were selected from 2596 common genes between the *E. coli* ST131 and BL21 strains (Table S3). The 77 genes that exhibited more than 4-fold up- or downregulation compared to SME98 are shown as orange or blue dots, respectively. (b and c) Screening for *vafA*- or *vafB*-regulated genes in the *E. coli* genome. Among the 77 genes with altered transcription levels after the acquisition of pIncI2_*mcr-1*, we further selected the genes that had attenuated transcription levels after deletion of *vafA* and/or *vafB*. (b) Distribution of transcription levels for the 77 genes. (c) Heatmap of the transcription levels of individual genes.

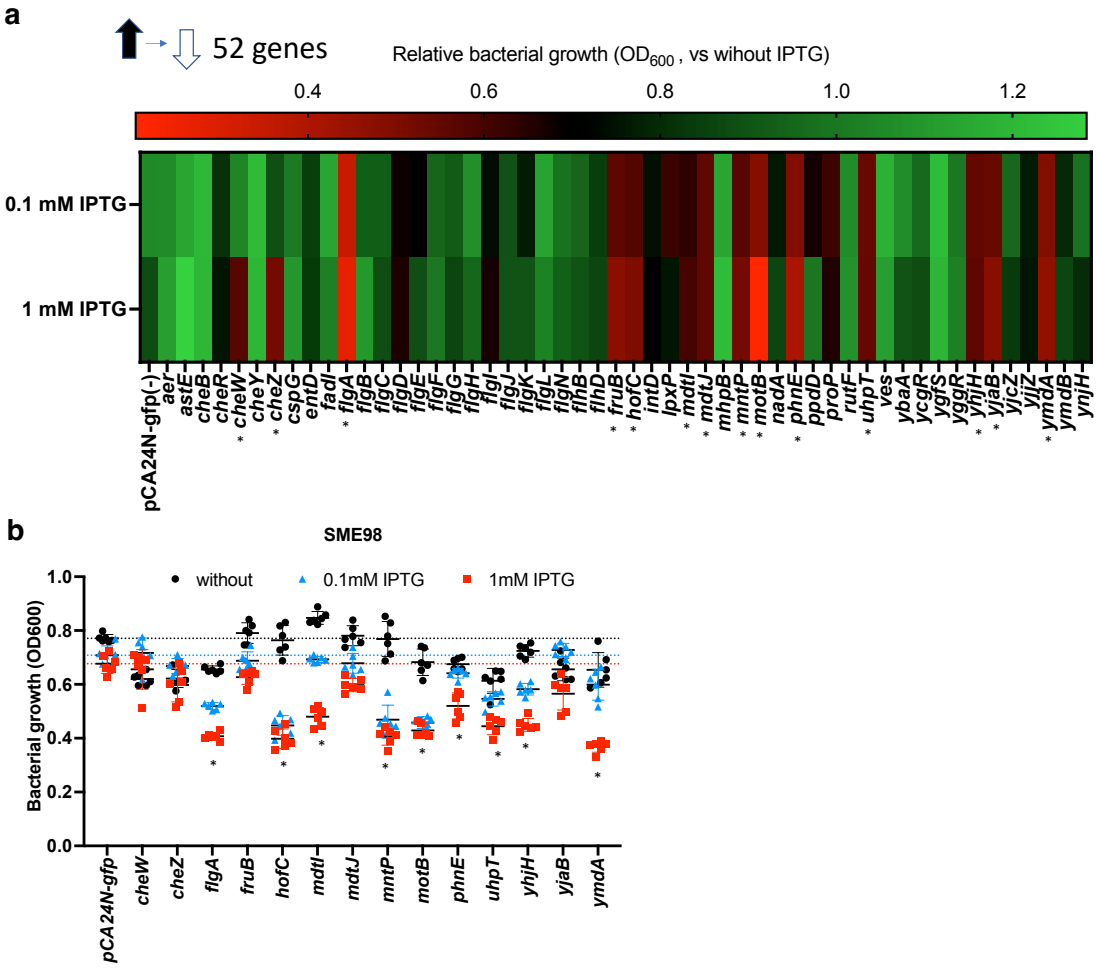

Extended Data Fig. 8 | Screening for growth inhibitory factors among upregulated genes after the acquisition of pIncI2_*mcr-1*. (a) Bacterial growth after expression of the 52 upregulated genes by using the *E. coli* ASKA clone library. The influence of 52 genes upregulated after the acquisition of pIncI2_*mcr-1* (but attenuated by the deletion of *vafA* and/or *vafB*, Extended Data Fig. 7c) on bacterial growth was evaluated in the *E. coli* AG1 strain for 16 h. These genes are strictly repressed by the *lacI* repressor located on pCA24N-gfp (+/-), and the encoding protein can be expressed via IPTG induction due to the presence of an IPTG-inducible promoter. * indicates a value < 0.6 for [0.1 or 1 mM IPTG (OD_{600})/without IPTG (OD_{600})] in the presence of 0.1 or 1 mM IPTG. (b) Influence of the protein expression of 14 selected upregulated genes on bacterial growth in ST131. We selected the 14 genes that attenuated the growth of *E. coli* AG1 in (a). The constructed gene-harbouring pCA24N vectors were introduced into *E. coli* SME98, and the encoded proteins were expressed via induction with 0.1 or 1 mM IPTG. The bacterial growth of *E. coli* SME98 was measured after 20 h of incubation at 37°C (OD_{600}). Bars indicate the average with standard deviation. * shows significant inhibition of growth in the presence of 0.1 and/or 1 mM IPTG (p <0.05 vs. without IPTG).

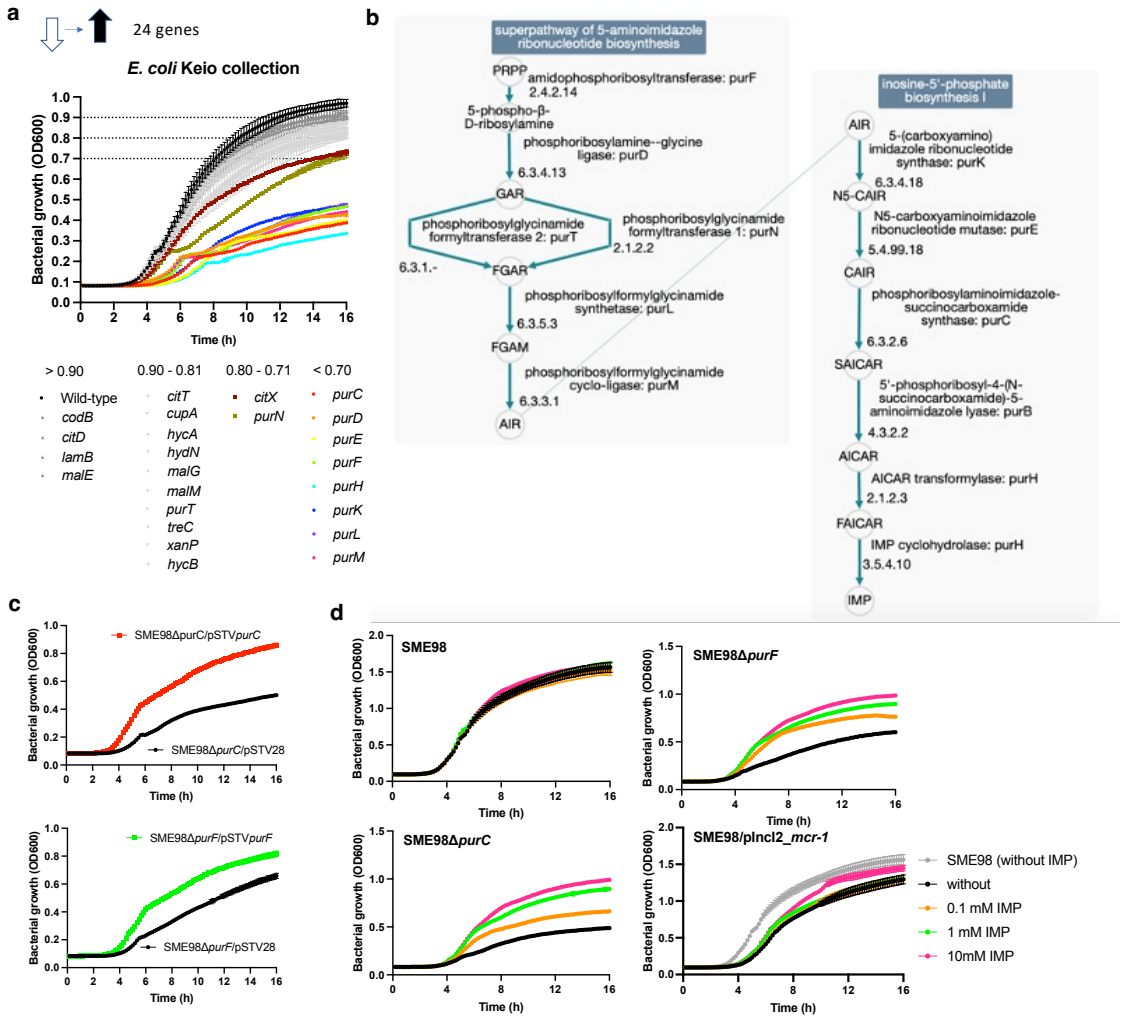

Extended Data Fig. 9 | Screening for growth inhibitory factors among the genes downregulated after the acquisition of pIncI2_*mcr-1*. (a) Bacterial growth after gene deletion of 24 downregulated genes by using the *E. coli* Keio collection. The influence of the 24 genes downregulated by the acquisition of pIncI2_*mcr-1* (and attenuated by the deletion of *vafA* and/or *vafB*) on bacterial growth (OD_{600}) was monitored in *E. coli* BW25113. The values obtained after 16 h of cultivation were classified as no significant change (> 0.90, dark grey), slight reduction (0.90-0.81, light grey), moderate reduction (0.80-0.71, coloured), or substantial reduction (<0.70, coloured) in growth. (b) Pathway analysis of *pur* genes by BioCyc. Left shows the super pathway of 5-aminoimidazole ribonucleotide biosynthesis, and right shows the inosine-5'-phosphate biosynthesis I pathway that is involved in nucleotide biosynthesis (purines). PRPP, 5-phosphoribosylpyrophosphate; GAR, glycinamide ribonucleotide; FGAR, N-formylglycinamide ribonucleotide; FGAM, N-formylglycinamidine ribonucleotide; AIR, aminoimidazole ribonucleotide; N^5-CAIR, N5-carboxyaminoimidazole ribonucleotide; CAIR, carboxyaminoimidazole ribonucleotide; SAICAR, N-succinocarboxamide-5-aminoimidazole ribonucleotide; AICAR, 5-aminoimidazole-4-carboxamide ribonucleotide; FAICAR, 5-formamido-4-imidazolecarboxamide ribonucleotide; IMP, inosine-5'-monophosphate. (c) Bacterial growth of *purC*- and *purF*-deletion mutants and their complementation mutants. *purC* or *purF* was cloned into pSTV28 with the -500 bp upstream region that includes the putative native promoter sequences. These *purC*- or *purF*- expression vectors were electroporated into *purC*- or *purF*-deletion SME98 mutants, respectively, and their bacterial growth was monitored. (d) Influence of inosine-5'-monophosphate on bacterial growth. We monitored the bacterial growth of SME98, the *purC*- and *purF*-deletion mutants, and SME98/pIncI2_*mcr-1* at 140 rpm and 37°C for 16 h in the presence of 0.1, 1, or 10 mM of inosine-5'-monophosphate (IMP).

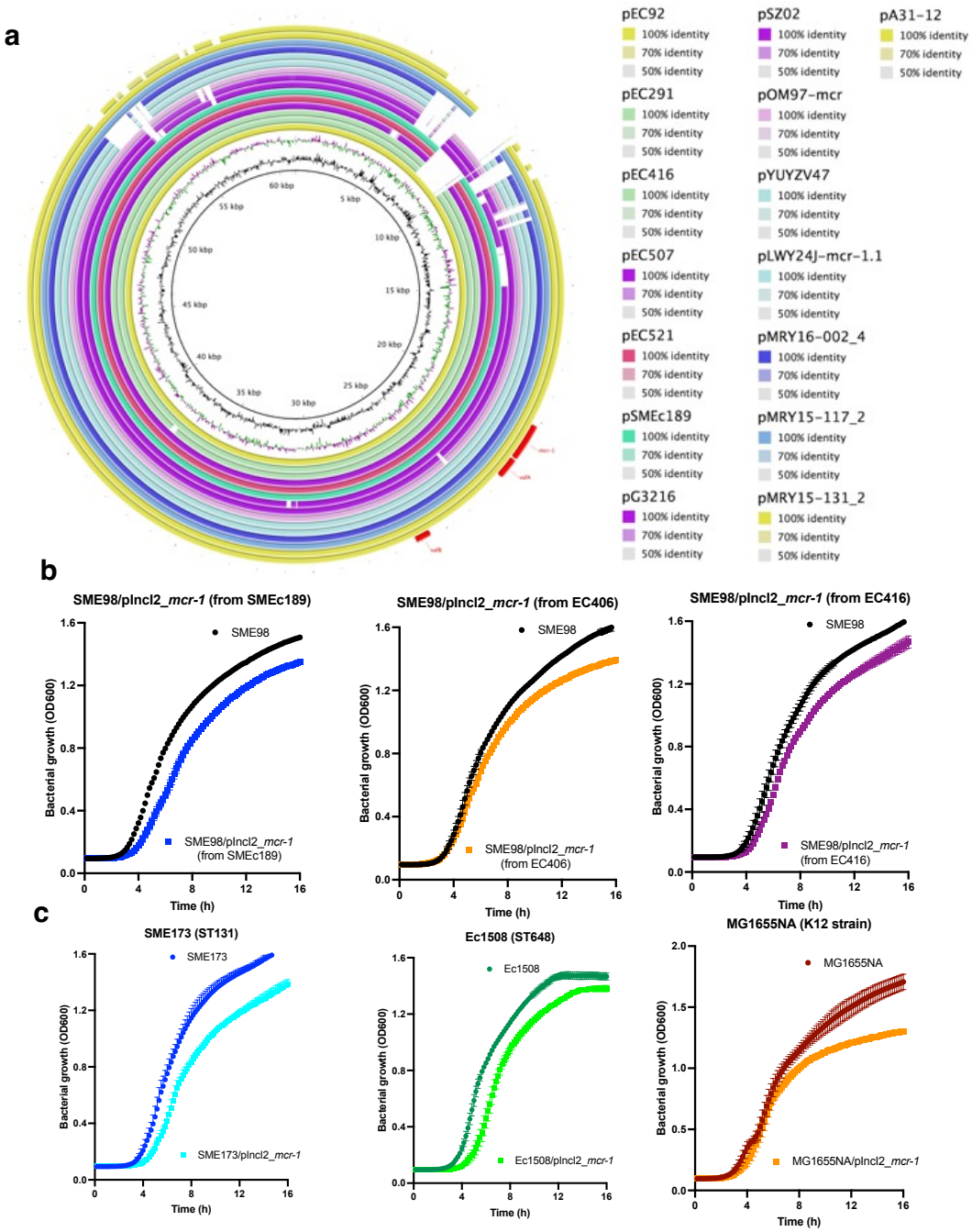

Extended Data Fig. 10 | Comparison of the influence of pIncI2_*mcr-1* on bacterial growth in *E. coli* isolates. (a) The nucleotide sequences of 14 representative pIncI2_*mcr-1* plasmids were obtained from NCBI and compared by BLAST RING. pIncI2_*mcr-1* from *E. coli* EC92 (pEC92) was used as a reference. Red arrows show *mcr-1*, *vafA*, and *vafB*. The presence of *vafA* and *vafB* in pIncI2_*mcr-1* plasmids is also listed in Table S4. (b) Influence of different pIncI2_*mcr-1* plasmids on the bacterial growth of ST131. Different pIncI2_*mcr-1* plasmids were transferred into the recipient strain (SME98) from donors (SMEc189, Ec406, and Ec416) via broth mating, and bacterial growth (OD_{600}) was monitored for 16 h at 37°C. (c) Influence of pIncI2_*mcr-1* on the growth of several E. coli clones. pIncI2_*mcr-1* from *E. coli* EC92 was transferred into three *E. coli* recipients of different lineages (SME173, Ec1508, and MG1655NA) via broth mating, and bacterial growth (OD_{600}) was monitored. MG1655NA is a nalidixic acid-resistant *E. coli* MG1655 mutant (the nalidixic acid MIC was >128 mg/L).